Phys Chem Minerals (2016) 43:209–216
DOI 10.1007/s00269-015-0787-0

ORIGINAL PAPER

Behaviour at high pressure of $Rb_7NaGa_8Si_{12}O_{40}\cdot 3H_2O$ (a zeolite with EDI topology): a combined experimental–computational study

G. D. Gatta[1,2] · G. Tabacchi[3] · E. Fois[3] · Y. Lee[4]

Received: 17 September 2015 / Accepted: 12 November 2015 / Published online: 10 December 2015

Abstract The high-pressure behaviour and the *P*-induced structural evolution of a synthetic zeolite $Rb_7NaGa_8Si_{12}O_{40}\cdot 3H_2O$ (with edingtonite-type structure) were investigated both by in situ synchrotron powder diffraction (with a diamond anvil cell and the methanol:ethanol:water = 16:3:1 mixture as pressure-transmitting fluid) up to 3.27 GPa and by ab initio first-principles computational modelling. No evidence of phase transition or penetration of *P*-fluid molecules was observed within the *P*-range investigated. The isothermal equation of state was determined; V_0 and K_{T0} refined with a second-order Birch–Murnaghan equation of state are $V_0 = 1311.3(2)$ Å^3 and $K_{T0} = 29.8(7)$ GPa. The main deformation mechanism (at the atomic scale) in response to the applied pressure is represented by the cooperative rotation of the secondary building units (SBU) about their chain axis (i.e. [001]). The direct consequence of SBU anti-rotation on the zeolitic channels parallel to [001] is the increase in pore ellipticity with pressure, in response to the extension of the major axis and to the contraction of the minor axis of the elliptical channel parallel to [001]. The effect of the applied pressure on the bonding configuration of the extra-framework content is only secondary. A comparison between the *P*-induced main deformation mechanisms observed in $Rb_7NaGa_8Si_{12}O_{40}\cdot 3H_2O$ and those previously found in natural fibrous zeolites is made.

Keywords Zeolite · $Rb_7NaGa_8Si_{12}O_{40}\cdot 3H_2O$ · High pressure · Compressibility · First-principles computational modelling

Introduction

The fibrous zeolites group is probably the most investigated one under extreme conditions. In particular, a series of experiments were devoted to this group of open-framework silicates at high pressure, in order to describe the elastic behaviour and the *P*-induced structural and chemical evolution at the atomic scale of these zeolites.

The crystal structure of "fibrous zeolites" is built on the 4 = 1 "secondary building units" (SBU, Gottardi and Galli 1985; Armbruster and Gunter 2001; Baerlocher et al. 2007), also known as "T_5O_{10} tetrahedral units". These units form chains running along [001] with tetragonal topological symmetry (Fig. 1), with different possible connectivity patterns, giving rise to the NAT (i.e. natrolite-type), THO (i.e. thomsonite-type) and EDI (i.e. edingtonite-type) topology (Smith 1983; Armbruster and Gunter 2001; Baerlocher et al. 2007; Gatta 2005). All the fibrous zeolites show a eight-membered ring channels system (hereafter 8mR[001]) parallel to the SBU-chain direction; additional eight-membered ring channels lie in the plane perpendicular to the SBU axis (hereafter 8mR[110]).

Electronic supplementary material The online version of this article (doi:10.1007/s00269-015-0787-0) contains supplementary material, which is available to authorized users.

✉ G. D. Gatta
diego.gatta@unimi.it

[1] Dipartimento di Scienze della Terra, Università degli Studi di Milano, Via Botticelli 23, 20133 Milan, Italy

[2] CNR - Istituto di Cristallografia, Sede di Bari, Via G. Amendola 122/o, Bari, Italy

[3] Dipartimento di Scienza e Alta Tecnologia, Università degli Studi dell'Insubria, Via Valleggio 9, 22100 Como, Italy

[4] Department of Earth System Sciences, Yonsei University, Seoul 120749, Korea

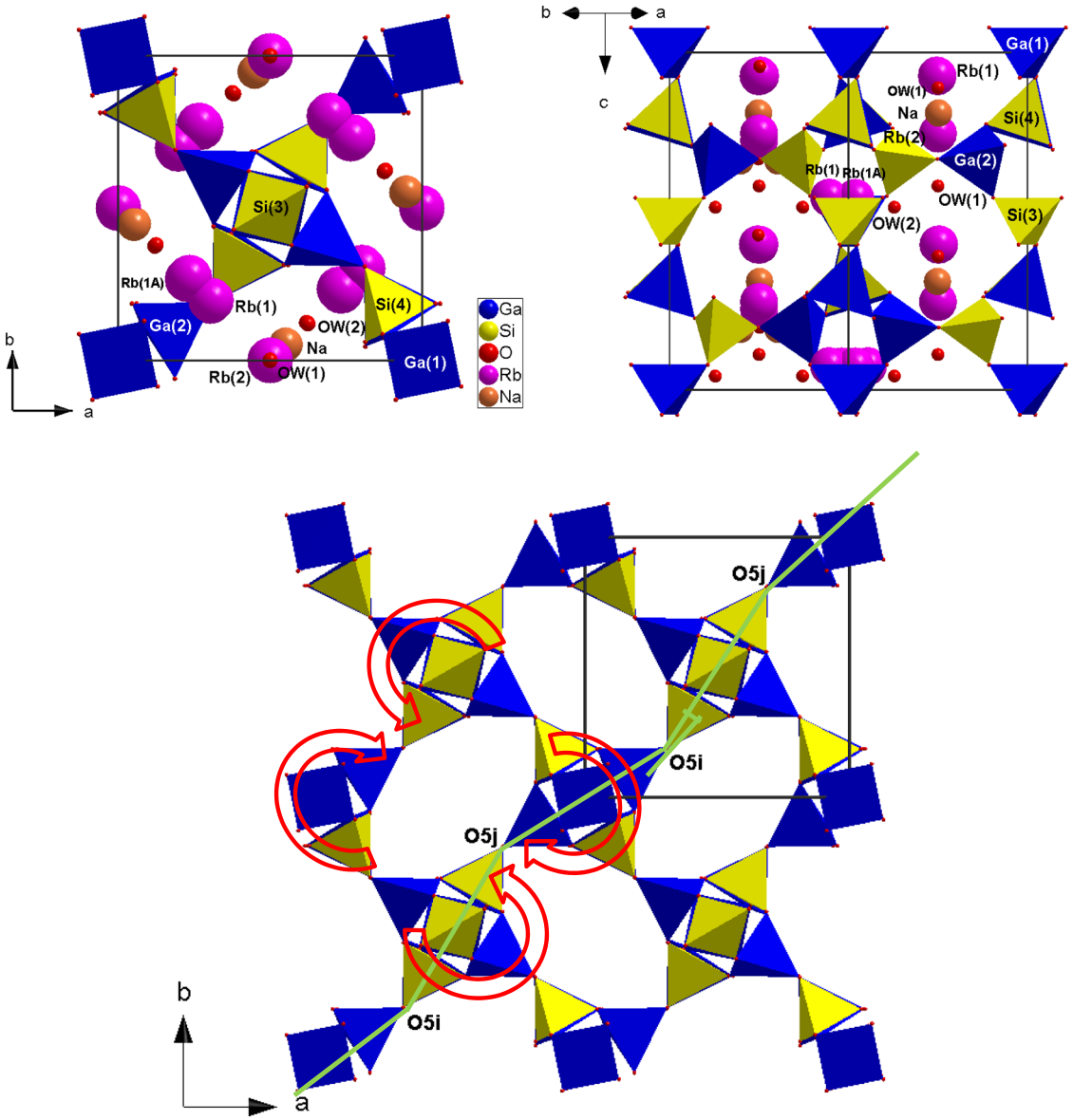

Fig. 1 Two views of the crystal structure of $Rb_7NaGa_8Si_{12}O_{40}{\cdot}3H_2O$ (i.e. down [001] and [110]), based on the structure model of Lee et al. (2000), along with the representation of the cooperative anti-rotation of the secondary building units in response to the applied pressure. The φ angle is also shown (see text for details)

The sodium member of this group, i.e. natrolite (ideally $Na_{16}Al_{16}Si_{24}O_{80}{\cdot}16H_2O$), was the first zeolite that showed unambiguously the so-called "pressure-induced hydration effect", through selective sorption of additional H_2O molecules from the *P*-transmitting fluid in response to the applied pressure (at ~1 GPa, using the methanol:ethanol:water = 16:3:1 mixture as *P*-transmitting fluid, Lee et al. 2002a). This phenomenon leads to formation of a new super-hydrated form of natrolite, with ideal chemical formula: $Na_{16}Al_{16}Si_{24}O_{80}{\cdot}32H_2O$. Recent investigations extended this discovery into other monovalent and divalent cation analogues of natrolites to establish that pressure-induced hydration is a systematic property of the natrolite framework materials (Seoung et al. 2013, 2015). On the basis of the compressibility paths of (natural) natrolite, scolecite (ideally $Ca_8Al_{16}Si_{24}O_{80}{\cdot}24H_2O$), thomsonite (ideally $Na_4Ca_8Al_{20}Si_{20}O_{80}{\cdot}24H_2O$), orthorhombic and tetragonal edingtonite (ideally $Ba_2Al_4Si_6O_{20}{\cdot}8H_2O$) obtained by in situ experiments, Gatta (2005) reported a comparative study on lattice compressibility, structural deformation mechanisms and the role played by the framework (Si/Al distribution, cross-linking of the building unit chains) and extra-framework content on the high-pressure behaviour of fibrous zeolites. Fitting the pressure–volume

data to an isothermal Birch–Murnaghan equation of state (Birch 1947), Gatta (2005) obtained an "average bulk modulus" of the fibrous zeolite (FZ) group: $K_{T0} = 50 \pm 10$ GPa. The bulk modulus value changes as a function of the extra-framework content, with: K_{T0}(Ba-FZ) > K_{T0}(Ca-FZ) > K_{T0}((Ca + Na)-FZ) > K_{T0}(Na-FZ) (Gatta 2005). In addition, comparing the in situ structure refinements available at that time (i.e. Lee et al. 2002a, b, 2004; Gatta et al. 2003, 2004a, b) and the structure models obtained by computational modelling (e.g. Ballone et al. 2002; Gatta and Wells 2004), Gatta (2005) showed how all the fibrous zeolites react with one main deformation mechanism in response to the applied pressure: the cooperative rotation (anti-rotation) of the SBU. This mechanism strongly reduces the free volume of the eight-membered ring channels parallel to the SBU-chain direction (Fig. 1).

Lee et al. (2000) reported the synthesis protocol and the crystal structures of gallium and germanium variants of the fibrous zeolites with the NAT, EDI and THO topology. In particular, the compound with ideal chemical formula $Rb_7NaGa_8Si_{12}O_{40}{\cdot}3H_2O$ showed the EDI-type structure, on the basis of a single-crystal X-ray structure refinement. The structure model of $Rb_7NaGa_8Si_{12}O_{40}{\cdot}3H_2O$ reported by Lee et al. (2000), described in the space group $P\text{-}42_1c$ with $a = 9.773(1)$ and $c = 13.141(3)$ Å (Fig. 1), consists of four independent tetrahedral sites (i.e. Ga(1), Ga(2), Si(3), Si(4), following the labelling scheme of Lee et al. 2000), five independent framework oxygen sites (i.e. O(1), O(2), O(3), O(4), O(5)), three independent rubidium sites with partial site occupancy (s.o.) [i.e. Rb(1) with s.o. 0.641(6), Rb(1A) with s.o. 0.093(4), Rb(2) with s.o. 0.278(7)], one sodium site [i.e. Na(2) with s.o. 0.139(8)] and two independent H_2O sites [i.e. OW(1) with s.o. 0.17(2), OW(2) with s.o. 0.33(2)]. Evidence of partial Si–Ga disorder was reported by Lee et al. (2000). The Ga–O bond distances were found ranging between 1.773(5) and 1.800(5) Å, whereas the Si–O distances between 1.616(5) and 1.648(5) Å. More complex is the reported coordination configuration of the extra-framework population: (1) With a maximum Rb(1)–O distance of 3.336(6) Å, the coordination number (C.N.) of Rb(1) is 10 (i.e. eight framework oxygen sites and two H_2O molecules); (2) Rb(1A) is coordinated by four framework oxygen sites, with a maximum Rb(1A)–O = 2.77(2) Å; (3) The C.N. is 7 for the Rb(2) site, with six framework oxygen sites and one H_2O molecule, with Rb(2)–O_{max} = 3.125(5) Å; (4) The C.N. of Na(2) is 6, with four framework oxygen sites and two H_2O molecules, with Na(2)–O_{max} = 3.02(5) Å. The C.N. of the Rb(1A) was likely underestimated by Lee et al. (2000), as its coordination shell might be better described with a longer Rb(1A)–O_{max} bond distance.

On the basis of our previous investigations on the high-pressure behaviour of fibrous zeolites, the aim of this study is to investigate the compressibility and the *P*-induced deformation mechanisms (at the atomic scale) of $Rb_7NaGa_8Si_{12}O_{40}{\cdot}3H_2O$ by in situ synchrotron X-ray powder diffraction with a diamond anvil cell and ab initio computational modelling. A comparison between the *P*-induced main deformation mechanisms observed in $Rb_7NaGa_8Si_{12}O_{40}{\cdot}3H_2O$ and those previously found in natural fibrous zeolites is made.

Experimental methods

The high-pressure experiments on $Rb_7NaGa_8Si_{12}O_{40}{\cdot}3H_2O$ were conducted using a polycrystalline sample synthesized by Lee et al. (2000). More details about the synthesis protocols and the crystallochemical characterization of this compound are given in Lee et al. (2000). In situ high-pressure synchrotron X-ray powder diffraction data were collected using a Merrill–Bassett-type diamond anvil cell (DAC) at the X14A beamline at the National Synchrotron Light Source (NSLS) at Brookhaven National Laboratory (BNL). The primary white beam from a bending magnet was horizontally monochromatized by Si(111) double crystals, in order to produce monochromatic X-ray with wavelength of 0.7745 Å. The polycrystalline sample was loaded into a 400-μm-diameter sample chamber in a pre-indented stainless steel gasket, along with a few small ruby spheres used as pressure markers. The mix methanol:ethanol:water = 16:3:1 was used as a (potentially penetrating) hydrostatic pressure-transmitting medium (Angel et al. 2007; Gatta 2008). The pressure at the sample was measured by detecting R_1 emission line of the ruby spheres in the DAC, following the protocol of Mao et al. (1986) (error in pressure estimated to be ± 0.1 GPa). High-pressure data were collected up to 3.27 GPa.

Unit-cell parameters were refined by Le Bail full-profile fit using the GSAS package (Le Bail et al. 1988; Larson and Von Dreele 2004; Table 1). The diffraction patterns were fitted using the pseudo-Voigt profile function

Table 1 Unit-cell parameters of $Rb_7NaGa_8Si_{12}O_{40}{\cdot}3H_2O$ measured at different pressure (*P*-uncertainty: ±0.1 GPa; unit-cell parameters at 0.0001 GPa after decompression differ by <4σ from those measured at room condition before compression). The wR_p of the Le Bail full-profile fits are listed

P (GPa)	*a* (Å)	*c* (Å)	*V* (Å^3)	wR_p
0.0001	9.9630(5)	13.2108(6)	1311.3(2)	0.0546
0.31	9.9405(4)	13.1924(5)	1303.5(1)	0.0523
0.94	9.8686(4)	13.1344(5)	1279.1(1)	0.0489
1.61	9.7716(4)	13.0616(5)	1247.2(1)	0.0645
2.39	9.6938(6)	13.0157(7)	1223.1(2)	0.0616
3.27	9.6121(4)	12.9480(5)	1196.3(1)	0.0486

of Thomson et al. (1987), and the background curve were refined with a Chebyshev polynomial. The quality of the high-pressure diffraction patterns hindered any attempt of structural refinement by Rietveld method (Rietveld 1969), and this led to use the ab initio computational modelling to describe the structure evolution (at the atomic scale) in response to the applied pressure.

Data collected after decompression showed that the compressional behaviour within the *P*-range investigated was completely reversible.

Computational modelling

First-principles molecular dynamics simulations were performed in order to study, at the atomistic level, the effects of compression on the title compound. The stoichiometry of the simulation cell is $Rb_7NaGa_8Si_{12}O_{40}{\cdot}3H_2O$.

The models were built by expanding the ambient conditions structure (described by Lee et al. 2000 in the space group $P\text{-}42_1c$) to $P1$, based on the unit-cell parameters measured at 0.0001, 0.94, 1.61 and 3.27 GPa, with: 20 independent tetrahedral sites (i.e. here labelled as T1a, T2a, T3a, T3b, T4a, T4b, T4c, T4d, T4e, T4f, T4g, T4h occupied by Si; T1b, T2b, T2c, T2d, T2e, T2f, T2g, T2h occupied by Ga); 40 framework oxygen sites (i.e. O1a-1h, O2a-2h, O3a-3h, O4a-4h, O5a-5h); seven rubidium sites (i.e. Rb1a-1e, Rb2, Rb3); one sodium site (i.e. Na); three H_2O sites (i.e. W1, W2a-2b); six hydrogen sites (i.e. H1-6) (see the CIFs, deposited as supplementary materials). The simulations were carried out at 300 K, with the Car–Parrinello approach (Car and Parrinello 1985). The electron–electron interactions were calculated by adopting the PBE approximation (i.e. Perdew–Burke–Ernzerhof) to the density functional theory (Perdew et al. 1996). Electron–nuclei interactions were accounted for via pseudopotential. In particular, norm-conserving pseudopotentials were adopted for Ga, Na, Rb and Si atoms (Troullier and Martins 1991), while ultra-soft pseudopotentials were adopted for O and H atoms (Vanderbilt 1990). Electronic wave functions were expanded in plane waves up to a kinetic energy cut-off of 25 Ry. A cut-off of 200 Ry was adopted for the representation of the electronic density. Simulations were performed in the canonical ensemble at fixed number of particles, fixed volume and fixed temperature. A Nose–Hoover thermostat was used for the temperature control (Hoover 1985). A time step of 5 atomic time unit was adopted for the integration of the equation of motion, and a fictitious inertia parameter of 500 atomic mass unit was adopted for the electronic wave function coefficient dynamics (e.g. Car and Parrinello 1985). All atoms in the simulations were considered independent, and only the unit-cell parameters were kept fixed at the experimental values. Such an approach was successfully used not only for the simulations of zeolitic and non-zeolitic systems at ambient conditions (e.g. Fois et al. 2008a, 2010a, 2012, 2013; Gamba et al. 2009; Gigli et al. 2014; Tabacchi et al. 2015) and at high temperature regimes (e.g. Ceriani et al. 2004; Fois et al. 2010b), but also for the investigation of high-pressure-induced processes in both natural and synthetic zeolites (e.g. Ferro et al. 2002; Arletti et al. 2003; Fois et al. 2005, 2008b; Betti et al. 2007). In the present simulations, for each compression degree, we have equilibrated the systems by performing molecular dynamics runs of 5 ps, while data were gathered and averaged from production runs of 12 ps. All calculations were performed using the CPMD computer code (CPMD 2015).

Results: Compressional behaviour

High-pressure unit-cell parameters of $Rb_7NaGa_8Si_{12}O_{40}{\cdot}3H_2O$ collected between 0.0001 and 3.27 GPa are summarized in Table 1, and their evolution with pressure is shown in Fig. 2. No phase transition was observed within the *P*-range investigated, although a nominally penetrating hydrous pressure medium was used in this experiment. We can therefore exclude any interference of the *P*-transmitting fluid in the *P*-behaviour of this zeolite. More specifically, any *P*-induced over-hydration effect (sensu Lee et al. 2002a; Gatta 2008) or penetration of methanol or ethanol molecules (from the *P*-transmitting fluid) can be ruled out. In fibrous zeolites, the *P*-induced penetration of external molecules through the channels leads to a drastic unit-cell volume expansion (Gatta 2005; Gatta and Lee 2014), which is not observed in this study.

Volume Eulerian finite strain versus normalized stress plot (f_E–F_E plot; $f_E = [(V_0/V)^{2/3}-1]/2$, $F_E = P/[3f_E(1+2f_E)^{5/2}]$) Angel 2000) is shown in Fig. 2. The weighted linear regression through the volume data points yields an almost horizontal trend, indicating that the compressional behaviour of this zeolite within the *P*-range investigated can be adequately described with a second-order Birch–Murnaghan equation of state (II-BM-EoS; Birch 1947; Angel 2000), as follows:

$$P(f_E) = 3K_{T0}f_E(1+2f_E)^{5/2},$$

where f_E is the Eulerian finite strain and K_{T0} is the bulk modulus, defined as the reciprocal of the volume compressibility coefficient (β): $\beta = 1/K_{T0} = V^{-1}\,\partial V/\partial P$.

P–*V* data were fitted with the EOS-FIT5.2 computer program (Angel 2000). The II-BM-EoS parameters obtained, using the weighted data by the uncertainties in *P*–*V*, are: $V_0 = 1311.3(2)$ Å^3, $K_{T0} = 29.8(7)$ GPa, $\beta = 1/K_{T0} = V^{-1}\,\partial V/\partial P = 0.0336(9)$ GPa^{-1}. A further fit performed without the measured V_0 gives: $V_0 = 1318(4)$

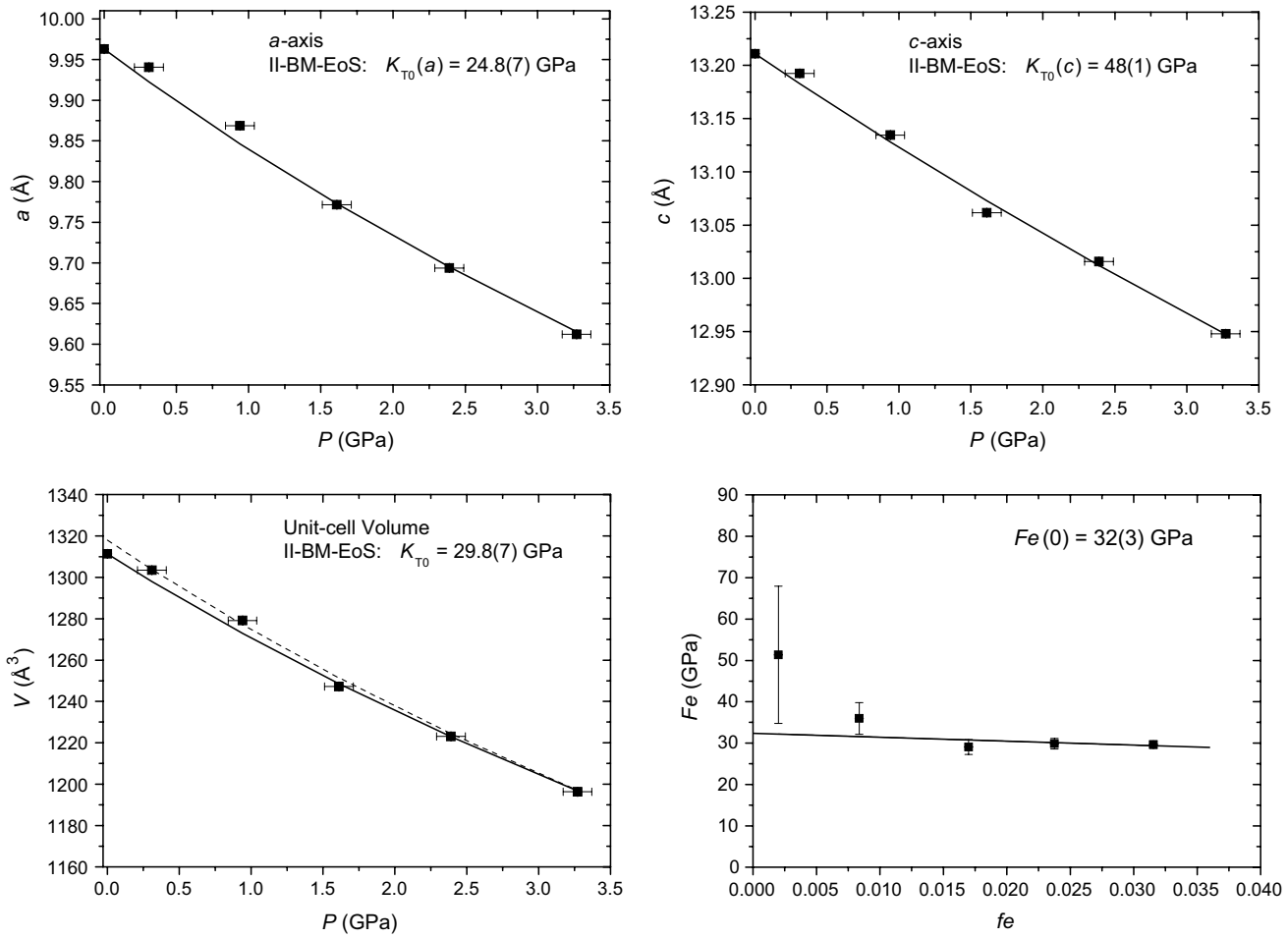

Fig. 2 Evolution of the unit-cell parameters of $Rb_7NaGa_8Si_{12}O_{40}{\cdot}3H_2O$ with pressure and Eulerian finite strain versus normalized stress plot (f_E–F_E plot). For the unit-cell parameters, the *solid lines* represent the Birch–Murnaghan equation of state fits; the *dotted line* for the unit-cell volume represents the fit without the measured V_0 (see text for further details)

Å^3, K_{T0} = 28(2) GPa. The second fit produces a better agreement between the observed and calculated *P*–*V* values and reflects the different operating conditions of the experiments: V_0 was measured without any *P*-medium in the DAC, and all the other *V* values at different pressures were measured with the *P*-fluid in the DAC. Similar evidence was often reported in the literature (e.g. Gatta 2005 and references therein).

The "axial bulk moduli" were calculated with "linearized" BM-EoS (Angel 2000), simply by substituting the cube of the individual lattice parameter (in this case: a^3 and c^3) for the volume. The refined elastic parameters obtained using a II-BM-EoS are: a_0 = 9.963(1) Å, $K_{T0}(a)$ = 24.8(7) GPa, $\beta(a) = l^{-1}\ \partial l/\partial P = (3K_{T0}(a))^{-1}$ = 0.0134(4) GPa^{-1} [fit without the measured a_0 gives: a_0 = 9.988(13) Å, $K_{T0}(a)$ = 22(1) GPa]; c_0 = 13.211(1) Å, $K_{T0}(c)$ = 48(1) GPa, $\beta(c) = l^{-1}\ \partial l/\partial P = (3K_{T0}(c))^{-1}$ = 0.0069(2) GPa^{-1} [fit without the measured c_0 gives: c_0 = 13.218(8) Å, $K_{T0}(c)$ = 46(2) GPa]. The elastic anisotropy of $Rb_7NaGa_8Si_{12}O_{40}{\cdot}3H_2O$ within the *P*-range investigated is: $K_{T0}(a)$:$K_{T0}(c) \approx 1{:}2$.

The diffraction data collected during decompression show that the structural modifications induced by the applied pressure are completely reversible (Table 1).

Results: Pressure-induced structure evolution

The pressure increase produces a slight variation on the intra-tetrahedral bond distances and angles, as deducible by the CIFs content. For example, the average T1a–O distance is 1.637 Å at 0.0001 GPa and 1.629 Å at 3.27 GPa (T1a was modelled as populated by Si); the average T2b–O distance is 1.721 Å at 0.0001 GPa and 1.718 Å at 3.27 GPa (T2b was modelled as populated by Ga). The tetrahedra distortion is, however, pronounced at any pressure, with differences between the longest and the shortest bond distances of ~0.05 Å.

The inter-tetrahedral tilting governs the most relevant deformation mechanisms. The main deformation mechanism is represented by a cooperative anti-rotation of the SBU along [001], causing the most prominent effects on (001) (Fig. 1). This mechanism produces a significant decrease in the O–O–O acute angles of the 8mR[001] (confining the channel along [001]) and, in contrast, an increase in the O–O–O obtuse angles. The direct consequence of SBU anti-rotation on the channels parallel to [001] is the increase in pore ellipticity with pressure, $\varepsilon_{8mR[001]}$, in response to the extension of the long diameters (i.e. the distance between the two oxygen atoms) and to the contraction of the short diameter O–O. Gatta et al. (2003, 2004a, b) suggested a way to quantify the effect of the SBU-chains anti-rotation by the evolution of the φ angle, shown in Fig. 1 and defined as $\varphi = [180-(<O5_i\text{-}O5_j\text{-}O5_i>)]/2$, where $<O5_i\text{-}O5_j\text{-}O5_i>$ is the average value of the $O5_i$-$O5_j$-$O5_i$ angles described by two connecting SBU. The φ angle value increases with increasing pressure, as shown in Table 2 and Fig. 3.

Table 2 Average φ angle (defined as: $\varphi = [180-(<O5_i\text{-}O5_j\text{-}O5_i>)]/2$, where $<O5_i\text{-}O5_j\text{-}O5_i>$ is the average value of the $O5_i$-$O5_j$-$O5_i$ angles described by two connecting SBU), ellipticity ratio of the eight-membered ring channels running along [001] (i.e. $\varepsilon_{8mR[001]}$) and along [110] (i.e. $\varepsilon_{8mR[110]}$). See text for further details

P (GPa)	φ (°)	$\varepsilon_{8mR[001]}$	$\varepsilon_{8mR[110]}$
0.0001	4.64	0.852	0.939
0.94	9.28	0.720	0.941
1.61	10.18	0.698	0.945
3.27	14.39	0.592	0.953

The shape of the 8mR[110] is nearly circular: its ellipticity ratio at room pressure approaches the unity (i.e. 0.939, Table 2). The evolution of $\varepsilon_{8mR[110]}$ is shown in Fig. 3, with a significant decrease in the ellipticity with increasing *P*. In other words, there is a regularization of the [110] channel shape with pressure: at the maximum pressure achieved in this experiment, the shape of 8mR[110] is not far away

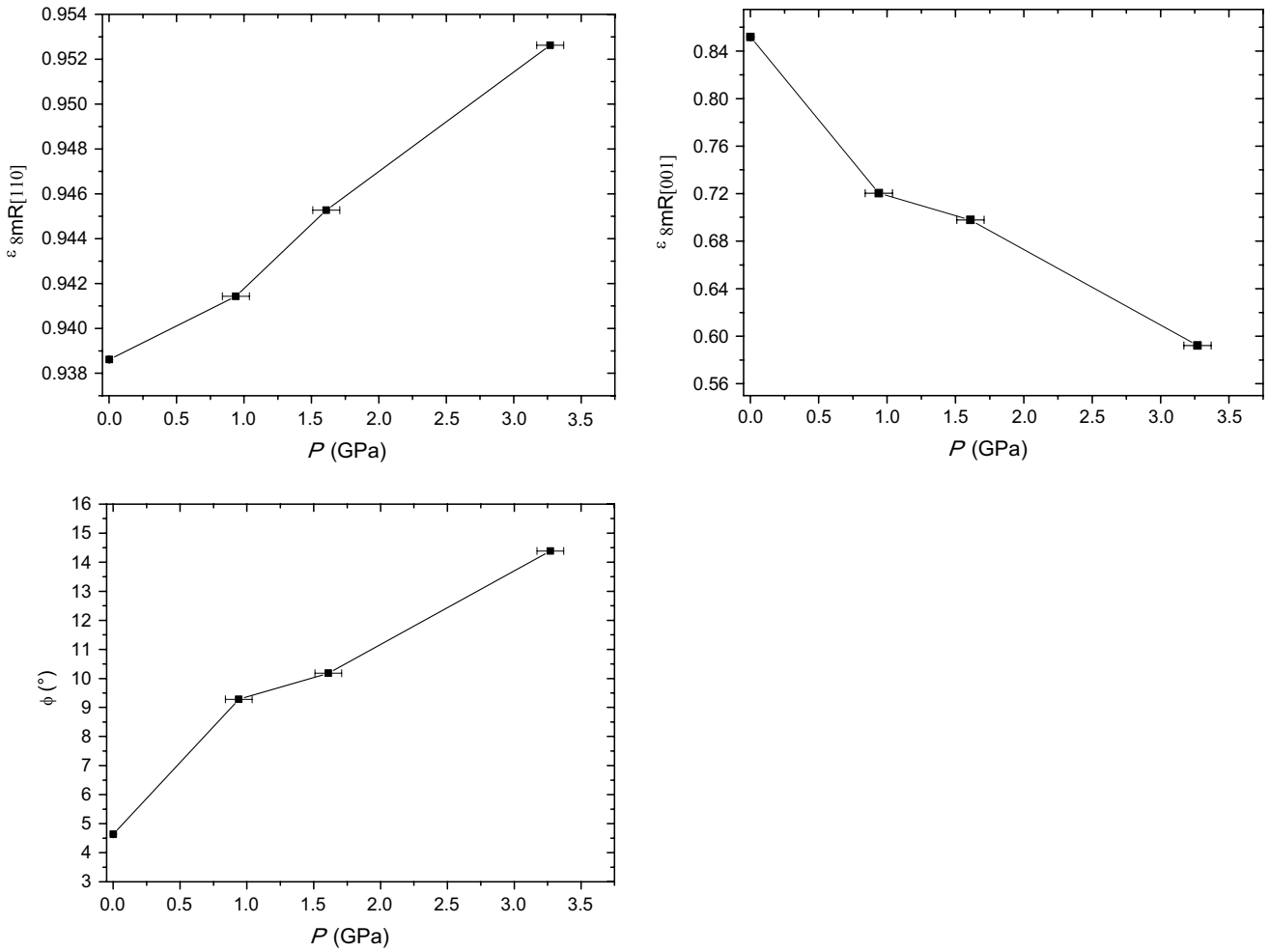

Fig. 3 Evolution of φ, $\varepsilon_{8mR[001]}$ and $\varepsilon_{8mR[110]}$ with pressure. The *error bars* represent the *P*-uncertainty

from the circularity (i.e. $\varepsilon_{8mR[110]} = 0.953$ at 3.27 GPa, Table 2). There is, therefore, an opposite behaviour of the two-channel systems in $Rb_7NaGa_8Si_{12}O_{40}{\cdot}3H_2O$ structure with *P*: the 8mR[001] channel tends to increase its ellipticity, whereas the 8mR[110] channel tends to decrease its ellipticity.

The effect of the applied pressure on the bonding configuration of the extra-framework content is only secondary, with no change of the coordination number.

Discussion and conclusions

The main deformation mechanism of $Rb_7NaGa_8Si_{12}O_{40}{\cdot}3H_2O$ under hydrostatic compression reflects the *P*-induced structural evolution observed in all the fibrous zeolites (Gatta 2005, 2010; Gatta and Lee 2014) and is represented by the anti-rotation of the SBU about the SBU-chain axis (i.e. [001]). This finding corroborates the conclusion of Gatta (2005): the SBU anti-rotation mechanism is independent of the nature of framework (i.e. elements that populate the tetrahedral sites and their ordering) and extra-framework content, and of the SBU-chains cross-linking geometry. The cooperative rotation of the SBU shows, in turn, that the flexibility of the tetrahedral framework under hydrostatic compression is mainly governed by tilting of (quasi-rigid) tetrahedra around oxygen atoms that behave as hinges within the framework, as observed in several classes of open-framework materials (Gatta 2010 and references therein). Due to the moderate *P*-range of this experiment, the tetrahedra compression and deformation are expected to be negligible.

As observed by Gatta et al. (2004b) in orthorhombic and tetragonal edingtonite, pressure-induced hydration effect is likely hindered by the extra-framework population. Also in this case, the 8mR[001] and 8mR[110] channels are already well stuffed at ambient conditions, leaving no room for additional H_2O (or methanol molecules) potentially able to penetrate through the channels. In contrast, in Na-, K- and Ca-bearing fibrous zeolites, the pressure-induced hydration effect occurs (e.g. Lee et al. 2002a, b; Colligan et al. 2005; Likhacheva et al. 2006, 2007), along with the *P*-induced penetration of other atoms or molecules (i.e. Ar, Xe or CO_2, Lee et al. 2010, 2011; Seoung et al. 2014). In this light, the extra-framework population does not control the main deformation mechanism of the framework, but can govern the general compressibility of the structure and the penetration of external atoms or molecules in response to the applied pressure. As a matter of fact, the bulk modulus of $Rb_7NaGa_8Si_{12}O_{40}{\cdot}3H_2O$ (i.e. $K_{T0} \sim 29$ GPa) is significantly lower than those observed for the natural fibrous zeolites (i.e. 43(2) for natrolite, 54.6(6) for scolecite, 49(1) for thomsonite, 59.3(4) for orthorhombic and tetragonal edingtonite; Gatta 2005). The higher compressibility of $Rb_7NaGa_8Si_{12}O_{40}{\cdot}3H_2O$ would only partially be attributed to the presence of Ga (replacing Al) in the tetrahedral framework: the channel content is likely responsible for the higher deformation of the structure under hydrostatic compression, if compared to the natural fibrous zeolites.

An interesting difference between the structural deformation mechanisms of $Rb_7NaGa_8Si_{12}O_{40}{\cdot}3H_2O$ and the isotypic (natural) edingtonite concerns the 8mR[110]. In $Rb_7NaGa_8Si_{12}O_{40}{\cdot}3H_2O$, there is a decrease in the ellipticity (i.e. a tendency to the circularity) with increasing pressure, whereas in the natural orthorhombic and tetragonal edingtonite, an increasing in ellipticity is observed with pressure (Gatta et al. 2004b). This difference is also ascribable to the different channel population (and its bonding configuration) between $Rb_7NaGa_8Si_{12}O_{40}{\cdot}3H_2O$ and the natural edingtonite.

Acknowledgments The authors thank the Italian Ministry of Education, MIUR-Project: "Futuro in Ricerca 2012-ImPACT- RBFR-12CLQD". Y. Lee thanks the Global Research Laboratory Program of the Korean Ministry of Science, ICT and Planning. Two anonymous reviewers are thanked.

References

Angel RJ (2000) Equation of state. In: Hazen RM, Downs RT (ed), High-temperature and high-pressure crystal chemistry, reviews in mineralogy and geochemistry. Mineralogical Society of America and Geochemical Society, Washington 41:35–59

Angel RJ, Bujak M, Zhao J, Gatta GD, Jacobsen SJ (2007) Effective hydrostatic limits of pressure media for high-pressure crystallographic studies. J Appl Crystallogr 40:26–32

Arletti R, Ferro O, Quartieri S, Sani A, Tabacchi G, Vezzalini G (2003) Structural deformation mechanisms of zeolites under pressure. Am Mineral 88:1416–1422

Armbruster T, Gunter ME (2001) Crystal structures of natural zeolites. In Bish DL, Ming DW (ed) Natural zeolites: occurrence, properties, application, reviews in mineralogy and geochemistry. Mineralogical Society of America and Geochemical Society, Washington 45:1–57

Baerlocher C, McCusker LB, Olson DH (2007) Atlas of zeolite framework types, 6th edn. Elsevier, Amsterdam

Ballone P, Quartieri S, Sani A, Vezzalini G (2002) High-pressure deformation mechanism in scolecite: a combined computational-experimental study. Am Mineral 87:1194–1206

Betti C, Fois E, Mazzucato E, Medici C, Quartieri S, Tabacchi G, Vezzalini G, Dmitriev V (2007) Gismondine under HP: deformation mechanism and reorganization of the extra-framework species. Microporous Mesoporous Mater 103:190–209

Birch F (1947) Finite elastic strain of cubic crystal. Phys Rev 71:809–824

Car R, Parrinello M (1985) Unified approach to molecular dynamics and density functional theory. Phys Rev Lett 55:2471–2474

Ceriani C, Fois E, Gamba A, Tabacchi G, Ferro O, Quartieri S, Vezzalini G (2004) Dehydration dynamics of bikitaite: Part II. Ab initio molecular dynamics study. Am Mineral 89:102–109

Colligan M, Lee Y, Vogt T, Celestian AJ, Parise JB, Marshall WG, Hriljac JA (2005) High pressure neutron powder diffraction study of superhydrated natrolite. J Phys Chem B 109:18223–18225

CPMD (2015) http://www.cpmd.org/, Copyright IBM Corp. 1990–2015, Copyright MPI für Festkörperforschung Stuttgart 1997–2001

Ferro O, Quartieri S, Vezzalini G, Fois E, Gamba A, Tabacchi G (2002) High-pressure behavior of bikitaite: an integrated theoretical and experimental approach. Am Mineral 87:1415–1425

Fois E, Gamba A, Tabacchi G, Arletti R, Quartieri S, Vezzalini G (2005) The "template" effect of the extra-framework content on zeolite compression: the case of yugawaralite. Am Mineral 90:28–35

Fois E, Gamba A, Tabacchi G (2008a) Bathochromic effects in electronic excitation spectra of hydrated Ti zeolites: a theoretical characterization. Chem Phys Chem 9:538–543

Fois E, Gamba A, Medici C, Tabacchi G, Quartieri S, Mazzucato E, Arletti R, Vezzalini G, Dmitriev V (2008b) High pressure deformation mechanism of Li-ABW: synchrotron XRPD and ab initio molecular dynamics simulations. Microporous Mesoporous Mater 115:267–280

Fois E, Tabacchi G, Calzaferri G (2010a) Interactions, behavior and stability of fluorenone inside zeolite nanochannels. J Phys Chem C 114:10572–10579

Fois E, Tabacchi G, Barreca D, Gasparotto A, Tondello G (2010b) "Hot" surface activation of molecular complexes: insight from modeling studies. Angew Chem Int Ed 49:1944–1948

Fois E, Tabacchi G, Calzaferri G (2012) Orientation and order of xanthene dyes in the one-dimensional channels of zeolite L: bridging the gap between experimental data and molecular behavior. J Phys Chem C 116:16784–16799

Fois E, Tabacchi G, Devaux A, Belser P, Brühwiler D, Calzaferri G (2013) Host–guest interactions and orientation of dyes in the one-dimensional channels of zeolite L. Langmuir 29:9188–9198

Gamba A, Tabacchi G, Fois E (2009) TS-1 from first principles. J Phys Chem A 113:15006–15015

Gatta GD (2005) A comparative study of fibrous zeolites under pressure. Eur J Mineral 17:411–422

Gatta GD (2008) Does porous mean soft? On the elastic behaviour and structural evolution of zeolites under pressure. Z Kristallogr 223:160–170

Gatta GD (2010) Extreme deformation mechanisms in open-framework silicates at high-pressure: evidence of anomalous inter-tetrahedral angles. Microporous Mesoporous Mater 128:78–84

Gatta GD, Lee Y (2014) Zeolites at high pressure: a review. Min Mag 78:267–291

Gatta GD, Wells SA (2004) Rigid unit modes at high pressure: an explorative study of a fibrous zeolite-like framework with EDI topology. Phys Chem Minerals 31:465–474

Gatta GD, Comodi P, Zanazzi PF (2003) New insights on high-pressure behaviour of microporous materials from X-ray single-crystal data. Microporous Mesoporous Mater 61:105–115

Gatta GD, Boffa Ballaran T, Comodi P, Zanazzi PF (2004a) Isothermal equation of state and compressional behaviour of tetragonal edingtonite. Am Mineral 89:633–639

Gatta GD, Boffa Ballaran T, Comodi P, Zanazzi PF (2004b) Comparative compressibility and equation of state of orthorhombic and tetragonal edingtonite. Phys Chem Minerals 31:288–298

Gigli L, Arletti R, Tabacchi G, Fois E, Vitillo JG, Martra G, Agostini G, Quartieri S, Vezzalini G (2014) Close-packed dye molecules in zeolite channels self-assemble into supramolecular nanoladders. J Phys Chem C 118:15372–15743

Gottardi G, Galli E (1985) Natural zeolites. Springer, Berlin

Hoover WG (1985) Canonical dynamics: equilibrium phase space distributions. Phys Rev A 31:1695–1697

Larson AC, Von Dreele RB (2004) General structure analysis system (GSAS), Los Alamos National Laboratory Report LAUR 86–748

Le Bail A, Duroy H, Fourquet JL (1988) Ab-initio structure determination of $LiSbWO_6$ by X-ray powder diffraction. Mater Res Bull 23:447–452

Lee Y, Kim SJ, Parise JB (2000) Synthesis and crystal structures of gallium- and germanium-variants of the fibrous zeolites with the NAT, EDI and THO structure types. Micropor Mesopor Mat 34:255–271

Lee Y, Vogt T, Hriljac JA, Parise JB, Artioli G (2002a) Pressure-induced volume expansion of zeolites in the natrolite family. J Am Chem Soc 124:5466–5475

Lee Y, Vogt T, Hriljac JA, Parise JB, Hanson JC, Kimk SJ (2002b) Non-framework cation migration and irreversible pressure-induced hydration in a zeolite. Nature 420:485–489

Lee Y, Hriljac JA, Studer A, Vogt T (2004) Anisotropic compression of edingtonite and thomsonite to 6 GPa at room temperature. Phys Chem Minerals 31:22–27

Lee Y, Hriljac JA, Vogt T (2010) Pressure-induced argon insertion into an auxetic small pore zeolite. J Phys Chem C 114:6922–6927

Lee Y, Liu D, Seoung D, Liu Z, Kao CC, Vogt T (2011) Pressure- and heat-induced insertion of CO_2 into an auxetic small-pore zeolite. J Am Chem Soc 133:1674–1677

Likhacheva A, Seryotkin Yu, Manakov A, Goryainov S, Ancharov A, Sheromov M (2006) Anomalous compression of scolecite and thomsonite in aqueous medium to 2 GPa. High Pres Res 26:449–453

Likhacheva AY, Seryotkin YV, Manakov AY, Goryainov SV, Ancharov AI, Sheromov MA (2007) Pressure-induced over-hydration of thomsonite: a synchrotron powder diffraction study. Am Mineral 92:1610–1615

Mao HK, Xu J, Bell PM (1986) Calibration of the ruby pressure gauge to 800 kbar under quasi-hydrostatic conditions. J Geophys Res 91:4673–4676

Perdew JP, Burke K, Ernzerhof M (1996) Generalized gradient approximation made simple. Phys Rev Lett 77:3865–3868

Rietveld HM (1969) A profile refinement method for nuclear and magnetic structures. J Appl Cryst 2:65–71

Seoung D, Lee Y, Kao CC, Vogt T, Lee Y (2013) Super-hydrated zeolites: pressure-induced hydration in natrolites. Chem Eur J 19:10876–10883

Seoung D, Lee Y, Cynn H, Park C, Choi KY, Blom DA, Evans WJ, Kao CC, Vogt T, Lee Y (2014) Irreversible xenon insertion into a small pore zeolite at moderate pressures and temperatures. Nat Chem 6:835–839

Seoung D, Lee Y, Kao CC, Vogt T, Lee Y (2015) Two-step pressure-induced superhydration in small pore natrolite with divalent extra-framework cations. Chem Mater 27:3874–3880

Smith JV (1983) Enumeration of 4-connected 3-dimensional nets and classification of framework silicates: combination of 4-1 chain and 2D nets. Z Kristallogr 165:191–198

Tabacchi G, Fois E, Calzaferri G (2015) Structure of nanochannel entrances in stopcock-functionalized zeolite L composites. Angew Chem Int Ed 54:11112–11116

Thomson P, Cox DE, Hastings JB (1987) Rietveld refinement of Debye–Scherrer synchrotron X-ray data from Al_2O_3. J Appl Cryst 20:79–83

Troullier N, Martins JL (1991) Efficient pseudopotentials for plane-wave calculations. Phys Rev B 43:1993–2006

Vanderbilt D (1990) Soft self-consistent pseudopotentials in a generalized eigenvalue formalism. Phys Rev B 41:7892–7895